ELSEVIER

Earth and Planetary Science Letters 198 (2002) 511–519

EPSL

www.elsevier.com/locate/epsl

Fossil pressures of fluid inclusions in mantle xenoliths exhibiting rheology of mantle minerals: implications for the geobarometry of mantle minerals using micro-Raman spectroscopy

Junji Yamamoto [a,b,*], Hiroyuki Kagi [a], Ichiro Kaneoka [b], Yong Lai [b,c], Vladimir S. Prikhod'ko [d], Shoji Arai [e]

[a] *Laboratory for Earthquake Chemistry, University of Tokyo, 7-3-1 Hongo, Bunkyo-ku, Tokyo 113-0033, Japan*
[b] *Earthquake Research Institute, University of Tokyo, 1-1-1 Yayoi, Bunkyo-ku, Tokyo 113-0032, Japan*
[c] *Department of Geosystem Engineering, University of Tokyo, 7-3-1 Hongo, Bunkyo-ku, Tokyo 113-8656, Japan*
[d] *Institute of Tectonics and Geophysics (Far-Eastern Branch, Russian Academy of Sciences), 65 Kim Yu Chen Str., Khabarovsk 680063, Russia*
[e] *Department of Earth Sciences, Faculty of Science, Kanazawa University, Kakuma, Kanazawa 920-1192, Japan*

Received 1 August 2001; received in revised form 14 January 2002; accepted 5 February 2002

Abstract

Micro-Raman spectroscopic analysis allows us to estimate the internal pressure of small fluid inclusions. We applied this method to CO_2-dominated fluid inclusions in mantle-derived xenoliths. The pressures estimated from the equilibration temperature and density of the fluid range from 0.96 to 1.04 GPa corresponding to depths of up to 30 km, which confirms that these rocks and fluids are of uppermost mantle origin. Furthermore, the inclusions show pressures specific to the individual host minerals (spinel $\geq$ orthopyroxene $\approx$ clinopyroxene $\gg$ olivine). In particular, the densities of CO_2 in pyroxenes are 10% higher than in olivine. Such an enormous difference cannot be explained by elastic deformation of the minerals during ascent of the xenoliths, although the process may explain the slightly higher density of CO_2 in spinel. During the ascent, the strain rate of orthopyroxene calculated using the 'constitutive equation' is several orders of magnitude lower than that of olivine. The difference in densities of CO_2 among the host mineral species is therefore attributable to the rheological properties of the minerals. Present internal pressures of fluid inclusions can be a sensitive strength marker of mantle minerals. Conversely, the density of CO_2 inclusions in pyroxene (and spinel) may be a useful geobarometer.

Keywords: geologic barometry; fluid inclusions; Raman spectroscopy; rheology; mantle; xenoliths

* Corresponding author. Tel.: +81-3-5841-5753; Fax: +81-3-5802-3391.
E-mail addresses: jyama@eqchem.s.u-tokyo.ac.jp (J. Yamamoto), kagi@eqchem.s.u-tokyo.ac.jp (H. Kagi), kaneoka@eri.u-tokyo.ac.jp (I. Kaneoka), lai@eri.u-tokyo.ac.jp (Y. Lai), vladimir@itig.khabarovsk.su (V.S. Prikhod'ko), ultrasa@kenroku.ipc.kanazawa-u.ac.jp (S. Arai).

0012-821X/02/$ – see front matter
PII: S0012-821X(02)00528-9

1. Introduction

The internal pressure of fluid inclusions in mantle-derived minerals can serve as a messenger from the deep Earth. For mantle-derived xenoliths, microthermometry of fluid inclusions has often been used to estimate the depth where the xenolith was entrained by host magma (e.g. [1–6]). For microthermometry, various technical difficulties lie in the use of small inclusions (smaller than 10 μm), multiple component fluid, metastable state, opaque minerals, and inclusions consisting of gas phase or liquid with low density. Although microthermometry is therefore the requisite tool to determine the density of the component in fluid inclusion, it is difficult to study variations of the internal pressure systematically in consideration of its occurrence. The advent of a new geobarometer applicable to mantle-derived materials with good accuracy and high spatial resolution has therefore been long awaited. Bertrán [7] admirably succeeded in determining the internal pressure of CO_2 fluid in a vessel by using Raman spectroscopy. The link between the Raman scale and density (pressure) of CO_2 fluid was also established [8–10]. The aim of this paper is to apply the Raman scale as a geobarometer to fluid inclusions in natural samples. There is a further point that needs to be clarified. Rheological properties of constituent minerals of the mantle have an important influence on geodynamics. For example, they are an important factor in controlling mantle convection and the depth variation of plastic properties may have implications for the origin of deep-focus earthquakes. Such rheological behavior of the constituent minerals may cause the deformation of the minerals during the ascent of the mantle-derived xenoliths. Consequently, the internal pressure of the inclusions may be affected by elastic or plastic deformation of the host minerals. To use fluid inclusions as a geobarometer, these effects should also be appraised. In this study, we have tried to develop a geobarometer applicable to mantle materials with good accuracy and high spatial resolution taking into account the influence of rheology on the internal pressure of fluid inclusions.

2. Samples and analyses

Several kinds of fluid are usually found as inclusions of mantle-derived minerals (e.g. H_2O, CO, N_2, CO_2 and noble gases (e.g. [11])). As most mantle-derived minerals contain CO_2 as a dominant component of fluid inclusion, micro-Raman spectra of CO_2 can serve as a geological barometer for fluid inclusion using CO_2 as molecular probe for pressure. The Raman spectrum of CO_2 has two main peaks of ν_+ (1388.0 cm^{-1}) and ν_- (1285.5 cm^{-1}), which are called a Fermi diad. They occur by an anharmonic interaction of the symmetric stretching mode (ν_1) with the overtone of the bending mode ($2\nu_2$). The intensity ratio ($I\nu_+/I\nu_-$, R) increases with pressure due to an enhancement of the intrinsic intensity of $2\nu_2$ with pressure [8,12,13]. The separation of wavenumber ($\nu_+ - \nu_-$, Δ) between the higher and the lower frequency peaks is also a function of pressure [7]. Further, the relationship between Δ and density of CO_2 is assumed to be linear [10,14]. Therefore, the combination of R and Δ may be used as a geobarometer. However, for natural samples, previous works have not adopted 'Δ' as a pressure marker [6,15–17].

In far eastern Siberia, many volcanisms have occurred since 20 Ma, and volcanic rocks contain abundant mantle-derived ultramafic xenoliths [18]. The present samples were taken from Ennokentiev which is in the middle of the Sikhote-Alin region, Russia. Four kinds of mineral separates (olivine, opx (orthopyroxene), cpx (clinopyroxene) and spinel) from two mantle-derived xenoliths (En1 and En2I (spinel–lherzolites)) were investigated in the present study. There are at least two compositionally distinct fluids as inclusions in the xenoliths. We defined inclusions in liquid or gas state and in solid state as liquid inclusion and melt one, respectively (Fig. 1a,b). The liquid inclusions are rarely >20 μm in size, and usually are <10 μm. As described in Section 3, the liquid inclusion is dominantly composed of CO_2. The melt inclusions are elongated vermicular ones, often forming a dendritic continuum. They would be filled with silicate melt.

Raman spectra were obtained on a 30 cm single

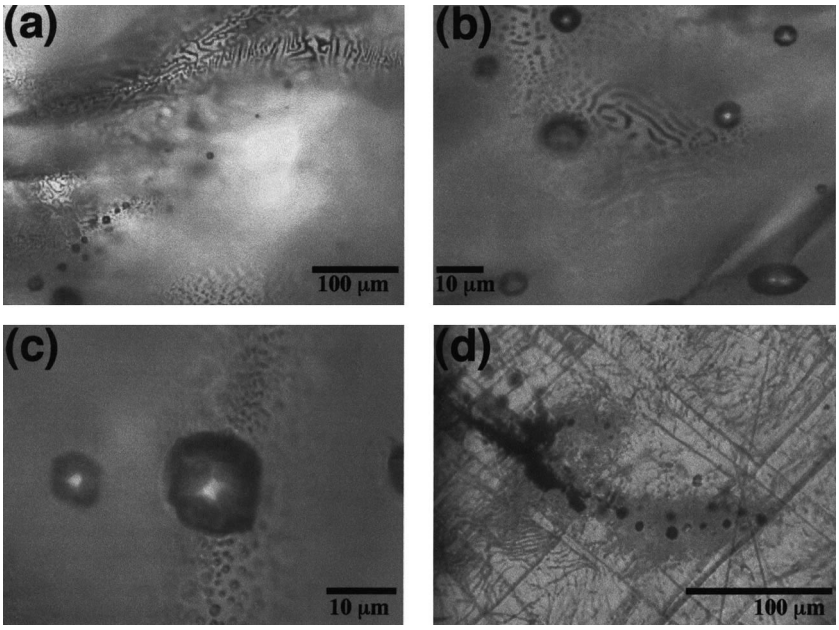

Fig. 1. Photomicrographs of xenolith thin slab (~300 μm) from far eastern Siberia. (a) Two generations of inclusions are visible in opx. The one is vermicular melt inclusions within a plane of the section. The other is indicated by liquid inclusion arrays. (b) Liquid inclusions in opx are penetrated by vermicular melt inclusions, and contain a vapor bubble, which showed Brownian motion. (c) Liquid inclusions in cpx. A central liquid inclusion, whose shape is negative crystal, is apparently penetrated by melt inclusions, which show a relatively low Δ value of approximately 105 cm^{-1} relative to other pyroxenes. (d) Dislocation structures in an olivine were observed with an optical microscope using the oxidation–decoration method [19]. High dislocation density is observed around the CO_2 inclusions.

polychromator (Chromex, 250is), equipped with an optical microscope (Olympus, BX60), Ar^+ laser (514.5 nm; ion laser technology, 5500 A), a CCD camera with 1024×256 pixels (Andor, DU420-OE) installed at the Laboratory for Earthquake Chemistry, University of Tokyo. The Rayleigh line was removed by using a holographic supernotch plus filter (Kaiser, HSPF-514.5-1.0). The excitation laser beam was focused on a spheroidal spot of approximately 1×1×5 μm in volume using an Olympus ×100 objective lens (NA = 0.95) with a confocal arrangement that allows us to pick up signals exclusively from fluid inclusions. Though the spectral resolution of our spectrometer is approximately 1.5 cm^{-1} per pixel at the present experimental condition, more than 20 data points are collected along the CO_2 Raman line, so the center of the fitted Lorentzian curve could be determined with much higher precision, typically ±0.15 cm^{-1} [20]. Spectra were accumulated with an exposure time of 10–100 s per point with laser power of 12–14 mW on the sample. There is a problem to be considered, which is the rise in internal pressure of the inclusion caused by the laser irradiation. This effect is dependent on laser power and beam size. It must be noted that our data of Δ and R may differ from those of other groups' experimental data, because the laser powers on samples differ from each other. Another problem still exists. There is a possibility that the temperature (internal pressure) in inclusions varies among host mineral species by differences in thermal conductivity even applying a constant laser power. However, this effect is negligible. This is because the Δ values remained constant within the experimental uncertainty of 1 σ level (~0.15 cm^{-1}) irrespective of the variation of laser power on the sample ranging from 3 to 14 mW for both olivine and opx. Within the range, also the intensity ratio of the summed intensities of the hot band diad to the summed intensities of the ν_1–$2\nu_2$ Fermi diad bands, which is

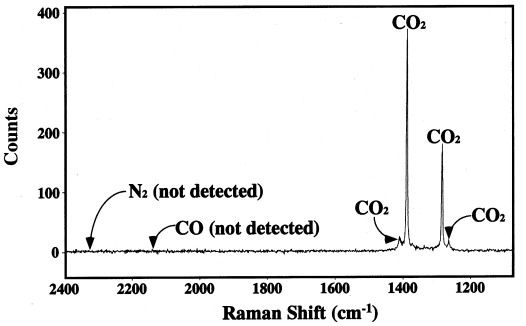

Fig. 2. Raman spectra of fluid inclusion. Only two narrow peaks for CO_2 are observed. No Raman signals occur for N_2 (2331 cm^{-1}) and CO (2140 cm^{-1}).

a definite indicator of temperature of CO_2 fluid [10], did not show a statistical correlation with laser power. These results imply that the present experimental condition did not cause any considerable artifact to the obtained R–Δ values.

Based on Raman microscopic analyses, CO_2 was identified in the liquid inclusions (Fig. 2). Beside CO_2, only C (graphite) was rarely detected on the wall of the CO_2 inclusions. Other components such as CH_4, H_2O, N_2 and CO were not detected. Because the liquid inclusions consist mostly of CO_2, a plot of R vs. Δ for the CO_2 Fermi diad by Raman spectroscopic analyses can be applied to estimate the internal pressures of the CO_2 inclusions.

3. Results and discussion

3.1. R–Δ plot for the CO_2 Fermi diad

Fig. 3 shows plots of R vs. Δ. Internal pressure of CO_2 increases toward the upper right direction along the lines. The inclusion data plot close to a line for the gas phase proposed by Bertrán [7], but it might be because CO_2 was transformed into the supercritical state during laser irradiation beyond the critical point of CO_2 (31.1°C). Overall, there is no systematic difference in internal pressure between the two samples, and the R–Δ plots are roughly separated into five regimes: spinel, pyroxene, olivine, fluid inclusion coexisting with vapor bubbles and gas state indicating a low Δ regime. The CO_2 inclusions in spinels show the highest Δ values among them, and those in pyroxenes follow. Those in olivines show relatively low Δ values. This gradation in present internal pressure between olivine and spinel+pyroxenes certainly occurs beyond the spectral resolution in the present study. This is because the wavenumbers of the Fermi diad were precisely determined with a resolution enhancement technique as described in Section 2. Since such a gradation of present internal pressure between olivine and pyroxenes was also reported by microthermometry for other mantle-derived xenoliths [4], it may be a general phenomenon for mantle-derived xenoliths, while the inclusions having vapor bubbles are plotted on an area of low Δ value irrespective of the samples or mineral species. Furthermore, there are many inclusions showing definitely lower Δ values than the inclusions having vapor bub-

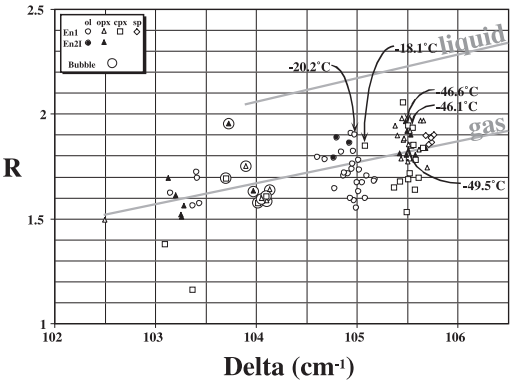

Fig. 3. R–Δ plot for the CO_2 Fermi doublet of CO_2 inclusions in several mineral species with data of homogenization temperatures of CO_2 in five inclusions, which are shown by arrows. R is the intensity ratio of the CO_2 Fermi diad. Δ is the separation of wavenumber of the CO_2 Fermi diad. The symbols of inclusions containing vapor bubbles are surrounded with a circle. The homogenization temperature was analyzed for five CO_2 inclusions in olivine, opx and cpx from a xenolith of En1. An inclusion in a cpx showed a low homogenization temperature of −18.1°C. This may be explained by partial loss of CO_2, because it was observed that this inclusion was penetrated by many μm-size melt inclusions (Fig. 1c). The reproducibility of the homogenization temperature was approximately ±0.2°C estimated by triple analyses of the same CO_2 inclusion. The reproducibility of Δ and R for data with moderate intensity (counts) is typically ∼0.15 cm^{-1} and ∼0.2, respectively. Because inclusions with low Δ values have a lower density than those with high Δ values, the data tend to show wide variation particularly in the R value.

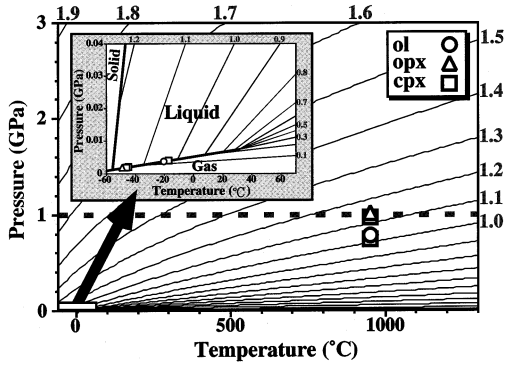

Fig. 4. *P–T* phase diagram of CO_2 with data of five CO_2 inclusions. Data of the equation of state for CO_2 are after Pitzer and Sterner [23]. Contours represent density, in g/cm^3 (i.e. isochores).

bles. Observations under an optical microscope indicate that inclusions that have Δ values irrespective of mineral species were obviously decrepitated or penetrated by melt inclusions. Therefore, such low Δ values would be attributed to partial loss of CO_2 from the inclusion by decrepitation or intrusion of the melt inclusions, then the inclusions plotting on the lowest Δ regime would consist of vapor phase. For the CO_2 inclusions penetrated by melt inclusions, the difference in Δ value between the inclusions with visible gas bubbles and those filled with CO_2 in the gas state would be attributed to the difference in degree of dissolution of CO_2 into the melt, while the inclusions showing Δ values specific to individual mineral species do not show such secondary effects. These results indicate that the original fluid trapped in the mantle was mostly retained as liquid CO_2 showing specific Δ values, and it is certain that the results of the Raman spectroscopic analyses reflect the difference in internal pressure of the CO_2 inclusions among mineral species.

3.2. Density of the CO_2

In order to give an absolute pressure scale to the Δ value, it is required to measure the density of the CO_2 in the present fluid inclusions. Assuming the composition to be pure CO_2, which was confirmed by our micro-Raman measurements, an accurate density of CO_2 can be determined by cryogenic microthermometry. The homogenization temperature at which the CO_2 inclusion of biphase (liquid and vapor) becomes homogenized to a single phase on heating gives the absolute value of density (see Fig. 4 and Table 1). The temperatures ranging from −18.1°C to −49.5°C correspond to the density of CO_2 ranging from 1.03 to 1.14 g/cm^3. Assuming that the relationship between Δ value and density of the CO_2 is linear in this density range, it is expressed as:

$$\Delta\ (\mathrm{cm}^{-1}) = 4.952 \times \mathrm{Density}\ (\mathrm{g/cm}^3) + 99.91 \quad (1)$$

Since spinel is opaque, the homogenization temperature of CO_2 fluid in spinel could not be measured. However, by using Eq. 1, we can obtain the density of CO_2 fluid in spinel. It is estimated to be 1.18 g/cm^3, which slightly exceeds that of the triple point of CO_2. The relationship of Eq. 1 is slightly different from the experimental data reported by other groups [8–10]. For instance, assuming a relationship proposed by Rosso and Bodnar [10], densities of CO_2 fluid in spinel, pyroxene and olivine are estimated to be 1.21, 1.14 and 0.95 g/cm^3, respectively, while our data are estimated to be 1.18, 1.14 and 1.04, respectively. The difference could be caused by considerable differences of laser power and beam size, which raise the internal pressure of inclusions, or systematic interlaboratory deviations on the energy

Table 1
Δ and density data for CO_2 inclusions in several mineral species

Sample	Host mineral	Δ cm^{-1}	Density g/cm^3	Homogenization temperature °C
en18251	olivine	104.98 ± 0.14	1.04	−20.2
en182835	opx	105.52 ± 0.13	1.14	−49.5
en18291	cpx	105.08 ± 0.13	1.03	−18.1
en182859	cpx	105.55 ± 0.14	1.13	−46.1
en182860	cpx	105.51 ± 0.14	1.13	−46.6

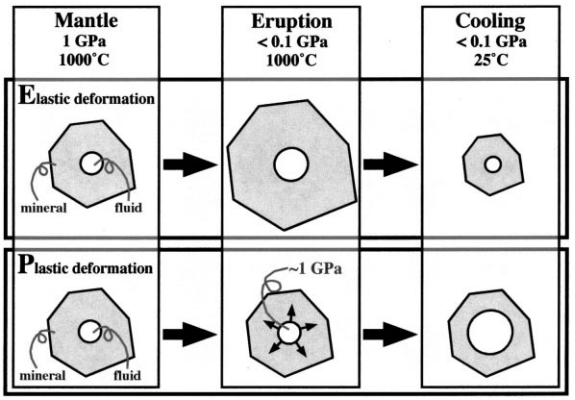

Fig. 5. Schematic illustrating two deformation models for constituent minerals of mantle xenolith. The xenolith is entrained by host magma to the Earth's surface in isothermal processes. On an elastic model, during the ascent of xenolith from a depth of 1 GPa (and 1000°C), the constituent minerals expand, and shrink with a decrease in temperature, while, when host basalt entrains the xenoliths to near the Earth's surface, CO_2 inclusions can keep pressures as high as those at the time of trapping. Hence, on a plastic model, differential stress up to several hundreds of MPa would have occurred between the CO_2 inclusion and surrounding crystal lattice. Thus the CO_2 inclusions may expand.

calibration of a detector. Trapping pressure of the xenoliths is given by the intersection of the isochore of CO_2 and the equilibration temperature of the xenoliths in the mantle. The equilibration temperature estimated from the two-pyroxene geothermometer [21] is approximately 950°C [22]. Hence, CO_2 pressures at the temperature can be calculated using the equation of state for CO_2 [23] at a temperature of 950°C. Extrapolation of the density of 1.04 g/cm^3 to higher temperatures indicates that the internal pressure of inclusions corresponds to about 0.8 GPa at 950°C (Fig. 4). Furthermore, adopting the highest density range of 1.13–1.14 g/cm^3, the internal pressure is estimated to have ranged from 0.96 to 1.04 GPa at 950°C. Such a pressure corresponds to 30 km or more in depth. Geophysical estimates indicate a relatively thin crustal thickness of $\sim$30 km for far eastern Siberia [24] and $\sim$34 km for the southern part of far eastern Siberia [25]. Therefore, the xenoliths may have been derived from the uppermost part of the mantle beneath the Siberia.

3.3. Cause of difference in Δ value among minerals

The liquid CO_2 inclusions in each mineral showed systematically different internal pressures (spinel $\geq$ opx $\approx$ cpx $\gg$ olivine). The CO_2 inclusions in olivines have a density of CO_2 lower than those of pyroxenes by about 10%. Thus, there is a possibility that the inclusions, especially those in olivine, do not reflect the internal pressure of the original fluid trapped at a depth in the mantle. These rocks are expected to have been crystallized and settled in the mantle. Therefore, it is difficult to explain the difference in CO_2 density among minerals by the difference in trapping depth of the fluid among minerals. The relatively low density of CO_2 in olivine may be attributed to its selective deformation during ascent of the xenoliths to the Earth's surface. Fig. 5 illustrates two deformation models for constituent minerals of xenolith during the ascent. Firstly, we have simulated the volume change of minerals caused by decompression and a decrease in temperature during the ascent based on differences in thermal expansivity and bulk modulus. The volume change of minerals can be calculated using both 'Birch–Murnaghan's equation of state' and 'thermal expansivities of minerals'. Thermal expansivity and bulk modulus are from Ahrens [26] and Saxena et al. [27]. During the ascent of xenoliths from the depth of 1 GPa ($\sim$30 km), the constituent minerals expand by approximately 1 vol%, and shrink by a few percent with a decrease in temperature due to the thermal expansion. This indicates that the volumes of inclusions (or densities of CO_2) are almost constant within a few percent with those prior to entrainment of the xenoliths, though the process may explain slightly high density of CO_2 fluid in spinel. The distinction is worth a mention in passing, because it would be useful to estimate the precise effect of the bulk modulus and thermal expansion. The above simulation indicates that olivine is more shrinkable than the other constituent minerals during the ascent and cooling of the xenoliths. Thus the inclusions in olivine would be compressed more. Therefore, such a process alone may not explain the difference in the internal pressures among minerals.

Kirby and Green [28] have suggested that oliv-

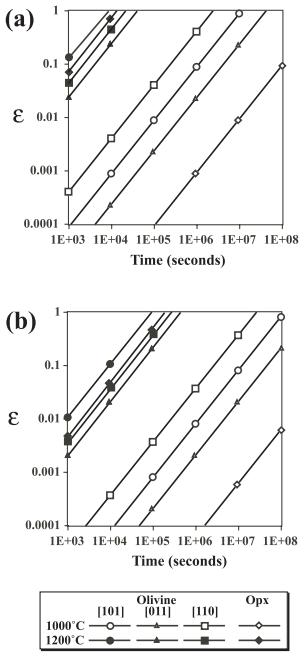

Fig. 6. Calculated strain of olivine (Fo = 91; [101], [011], [110]) and orthopyroxene ($Mg^{\#} = 96.2$) as a function of time scale and temperature under conditions of oxygen fugacity of 10^{-16} MPa, temperature of host basalt of both 1000°C and 1200°C. Differential stresses are 1 GPa (a) and 0.5 GPa (b). Average strain rate of three axes should be applicable to the expansion of CO_2 inclusion in olivine.

ine can easily deform plastically during eruption, because transmission electron micrographs of some inclusions of olivine show dislocation loops indicating expansion. During the entrainment of xenoliths to near the Earth's surface, CO_2 inclusions can keep internal pressures as high as those prior to the entrainment [11]. Thus, differential stress up to 100 MPa would have occurred between the CO_2 inclusion and surrounding crystal lattice.

The CO_2 inclusions in olivines have a density of CO_2 lower than those of opx by about 10%. If the relatively low density of CO_2 in olivine was attributed to its selective plastic deformation, it followed that the diameter of CO_2 inclusions in olivine has decreased by about 3%. Further, given that the deformation occurred for 10 days, the strain rate is estimated to be about 3×10^{-8} s^{-1}. The time scale of 10 days might be reasonable for annealing the xenoliths, because it corresponds to the order of the time scales estimated by the rate of decrease in dislocation density of olivine [29]. In order to confirm the plastic deformation model, we have simulated the volume change of CO_2 inclusion in both olivine and opx caused by the plastic deformation. The volume change was calculated using the 'constitutive equation' (e.g. [30]). The volume changes of olivine and opx were calculated using the 'constitutive equation' suggested by Bai et al. [31] and Mackwell [32], respectively. Fig. 6 shows the strain of the minerals as a function of time scale and temperature under conditions of oxygen fugacity of 10^{-16} MPa, temperature of host basalt of both 1000°C and 1200°C, and differential stress of both 1 GPa and 0.5 GPa. Since the differential stress of 1 GPa should be close to a maximum, actual differential stress may be several hundreds of MPa. Thus both 1 GPa and 0.5 GPa were adopted in Fig. 6. The oxygen fugacity around the CO_2 inclusion may be restricted by the chemical equilibrium '$C+O_2 = CO_2$', because graphite was observed in some CO_2 inclusions. Oxygen fugacity of pelitic metamorphic rock including graphite corresponds to the stability field of magnetite [33]. Hence the oxygen fugacity around the CO_2 inclusions may be similar to that of QFM (a system of quartz–fayalite–magnetite), thus $\sim10^{-16}$ MPa at around 1000°C. The xenoliths were trapped by host basalt that had a relatively high temperature. Therefore we adopted 1000°C and 1200°C for the calculation. At 1000°C, the strain rate of opx is several orders of magnitude lower than that of olivine (Fig. 6). Under the condition of 1200°C, opx becomes easy to deform plastically. However, the strength on plastic deformation of opx is closely related to the Mg# [Mg/(Fe+Mg)] [31]. The strength of present opx with Mg# of about 90 [22] should be several orders of magnitude higher than that used in the calculation. Thus, CO_2 inclusions in olivine selectively expand under the conditions. Indeed, significant high dislocation density is developed in olivine crystals around CO_2 inclusions (see Fig. 1d). Under the conditions of 1000°C and differential stress of 0.5 GPa, olivine would be deformed by a strain rate of about 4×10^{-8} s^{-1} along the [110] direction. This value is fairly similar to the above estimation. If such a

condition could have been kept for 10 days, the CO_2 inclusions in olivine would expand by 10% in volume. Since it would be regarded as a condition with a minimum of plastic deformation, the deformation of olivine occurred within 10 days. The more detailed estimation may allow us to constrain the time scale of ascent and cooling of the xenoliths. However, we have no definite information on these conditions. For this purpose, it becomes necessary to accumulate basic knowledge particularly on rheology of mantle minerals.

The density of CO_2 in liquid inclusions in spinel was the highest of all mineral species (Fig. 3), though the absolute density of CO_2 fluid in spinel could not be analyzed due to its opacity. Since spinel has considerably higher creep strength than olivine [34], the difference in density of CO_2 between spinel and pyroxenes may not be explained by the plastic deformation of these minerals. As calculated above, the spinel ($MgAl_2O_4$) is more shrinkable than both opx (orthoenstatite) and cpx (clinodiopside) during the ascent and cooling of xenoliths. Thus the inclusions in spinel would be compressed more, which is inconsistent with our observation. Therefore, the relatively higher density of CO_2 in liquid inclusions in spinel than in pyroxenes may be attributed to the elastic deformation of these minerals occurring during the ascent of the xenoliths.

In this study, it was shown that micro-Raman spectroscopy can throw light on measuring internal pressures of small fluid inclusions (>1 μm). As a possible geobarometer, Raman spectra of CO_2 fluid in inclusions in spinel, opx (and cpx) would be applicable for mantle-derived xenoliths. The difference in rheological character among mineral species is clearly revealed by the pressure of fluid inclusions obtained grain by grain.

4. Conclusions

From the R–Δ plot for the CO_2 Fermi diad by Raman spectroscopic analyses, the Δ value of the CO_2 inclusions decreases in the order: spinel, pyroxene, and olivine. From the lowest homogenization temperature of -49.5°C, the density of CO_2 is estimated to be approximately 1.14 g/cm^3. This indicates that the internal pressure was at least 1 GPa at a temperature of 950°C, which is lithostatically comparable to depths of up to 30 km.

The inclusions show pressures specific to the individual host minerals (spinel $\geq$ opx $\approx$ cpx $\gg$ olivine). In particular, the densities of CO_2 in pyroxenes are 10% higher than in olivine. From calculation of both elastic and plastic deformation of minerals, the relatively low density of CO_2 in olivine may be attributed to its plastic deformation during ascent of the xenoliths to the Earth's surface. The deformation of opx is several orders of magnitude smaller than that of olivine and thus the effect may be neglected. Also, spinel has higher creep strength than olivine [34]. Therefore, the density of CO_2 inclusions in pyroxene and spinel is suitable for a geobarometer. Conversely, present internal pressures of fluid inclusions can be a sensitive strength marker of mantle minerals.

Acknowledgements

We thank Professors Oded Navon, George R. Rossman and Masaaki Obata, who reviewed the manuscript and gave various useful comments on it. We would like to acknowledge Dr. K. Mibe for his useful suggestions on the calculation of the thermodynamics. Prof. K. Ozawa, Prof. M. Toriumi, Dr. J. Ando, Dr. Y. Takei and Dr. T. Yoshino gave constructive comments for the rheological calculation. We wish to express our deep appreciation to Prof. G.P. Glasby for his effort to correct English. This research was supported by a Grant-in-Aid (11304040, 13554018, 12640476) from the Ministry of Education, Science and Culture of Japan.*[AH]*

References

[1] E. Roedder, Liquid CO_2 inclusions in olivine-bearing nodules and phenocrysts from basalts, Am. Mineral. 50 (1965) 1746–1782.
[2] E. Roedder, Geobarometry of ultramafic xenoliths from Loihi Seamount, Hawaii, on the basis of CO_2 inclusions in olivine, Earth Planet. Sci. Lett. 66 (1983) 369–379.
[3] T. Andersen, S.Y. O'Reilly, W.L. Griffin, The trapped

fluid phase in upper mantle xenoliths from Victoria, Australia: implications for mantle metasomatism, Contrib. Mineral. Petrol. 88 (1984) 72–85.
[4] R.G. Schwab, B. Freisleben, Fluid CO_2 inclusions in olivine and pyroxene and their behaviour under high pressure and temperature conditions, Bull. Mineral. 111 (1988) 297–306.
[5] B. DeVivo, M.L. Frezzotti, A. Lima, R. Trigila, Spinel lherzolite nodules from Oahu island (Hawaii): a fluid inclusion study, Bull. Mineral. 111 (1988) 307–319.
[6] M.L. Frezzotti, E.A.J. Burke, B. DeVivo, B. Stefanini, I.M. Villa, Mantle fluids in pyroxenite nodules from Salt Lake Crater (Oahu, Hawaii), Eur. J. Mineral. 4 (1992) 1137–1153.
[7] J.F. Bertrán, Study of the Fermi doublet ν_1-$2\nu_2$ in the Raman spectra of CO_2 in different phases, Spectrochim. Acta 39A (1983) 119–121.
[8] Y. Garrabos, R. Tufeu, B.L. Neindre, G. Zalczer, D. Beysens, Rayleigh and Raman scattering near the critical point of carbon dioxide, J. Chem. Phys. 72 (1980) 4637–4651.
[9] Y. Garrabos, V. Chandrasekharan, M.A. Echargui, F. Marsault-Herail, Density effect on the Raman Fermi resonance in the fluid phases of CO_2, Chem. Phys. Lett. 160 (1989) 250–256.
[10] K.M. Rosso, R.J. Bodnar, Microthermometric and Raman spectroscopic detection limits of CO_2 in fluid inclusions and the Raman spectroscopic characterization of CO_2, Geochim. Cosmochim. Acta 59 (1995) 3961–3975.
[11] T. Andersen, E.-R. Neumann, Fluid inclusions in mantle xenoliths, Lithos 55 (2001) 301–320.
[12] R.B. Wright, C.H. Wang, Density effect on the Fermi resonance in gaseous CO_2 by Raman scattering, J. Chem. Phys. 58 (1973) 2893–2895.
[13] C.H. Wang, R.B. Wright, Raman studies of the effect of density on the Fermi resonance in CO_2, Chem. Phys. Lett. 23 (1973) 241–246.
[14] A. Hacura, A. Bródka, L. Nikiel, F.G. Baglin, High pressure Raman study of Fermi resonance spectrum in gaseous carbon dioxide, J. Mol. Struct. 218 (1990) 297–302.
[15] J.D. Pasteris, B.J. Wanamaker, Laser Raman microprobe analysis of experimentally re-equilibrated fluid inclusions in olivine: some implications for mantle fluid, Am. Mineral. 73 (1988) 1074–1088.
[16] A.M. van den Kerkhof, S.N. Olsen, A natural example of superdense CO_2 inclusions: microthermometry and Raman analysis, Geochim. Cosmochim. Acta 54 (1990) 895–901.
[17] J.C. Seitz, J.D. Pasteris, I.-M. Chou, Raman spectroscopic characterization of gas mixtures. II. Quantitative composition and pressure determination of the CO_2-CH_4 system, Am. J. Sci. 296 (1996) 577–600.
[18] D.A. Ionov, V.S. Prikhod'ko, S.Y. O'Reilly, Peridotite xenoliths in alkali basalts from the Sikhote-Alin, southeastern Siberia, Russia: trace-element signatures of mantle beneath a convergent continental margin, Chem. Geol. 120 (1995) 275–294.
[19] D.L. Kohlstedt, C. Goetze, W.B. Durham, J.B. Van der Sande, A new technique for decorating dislocations in olivine, Science 191 (1975) 1045–1046.
[20] E.S. Izraeli, J.W. Harris, O. Navon, Raman barometry of diamond formation, Earth Planet. Sci. Lett. 173 (1999) 351–360.
[21] P.R.A. Wells, Pyroxene thermometry in simple and complex systems, Contrib. Mineral. Petrol. 62 (1977) 129–139.
[22] J. Yamamoto, Investigation of the Subcontinental Mantle based on Noble Gas Isotopes, Petrological and Spectroscopic Studies of Siberian Mantle Xenoliths, PhD Thesis, University of Tokyo, Tokyo, 2001.
[23] K.S. Pitzer, S.M. Sterner, Equations of state valid continuously from zero to extreme pressures for H_2O and CO_2, J. Chem. Phys. 101 (1994) 3111–3116.
[24] B. Karp, E.P. Leikov, Geological structure, composition and evolution of crustal layers of the Japan Sea, Tectonophysics 181 (1990) 277–283.
[25] T. Zai-Yi, H. Ping, X. Ke-Ding, The Mesozoic-Cenozoic East China rift system, Tectonophysics 208 (1992) 341–363.
[26] T.J. Ahrens (Ed.), Mineral Physics and Crystallography: A Handbook of Physical Constants, American Geophysical Union, Washington, DC, 1995, 354 pp.
[27] S.K. Saxena, N. Chatterjee, Y. Fei, G. Shen, Thermodynamic Data on Oxides and Silicates, Springer-Verlag, New York, 1993, 428 pp.
[28] S.H. Kirby, H.W. Green, Dunite xenoliths from Hualalai volcano: evidence for mantle diapiric flow beneath the island of Hawaii, Am. J. Sci. 280-A (1980) 550–575.
[29] M. Toriumi, S. Karato, Experimental studies on recovery process of deformed olivines and the mechanical state of the upper mantle, Tectonophysics 49 (1978) 79–95.
[30] J.-P. Poirier, Creep of Crystals, Cambridge University Press, Cambridge, 1985, 260 pp.
[31] Q. Bai, S.J. Mackwell, D.L. Kohlstedt, High-temperature creep of olivine single crystals 1. mechanical results for buffered samples, J. Geophys. Res. 96 (1991) 2441–2463.
[32] S.J. Mackwell, High-temperature rheology of enstatite: implications for creep in the mantle, Geophys. Res. Lett. 18 (1991) 2027–2030.
[33] A. Miyashiro, Oxidation and reduction in the Earth's crust with special reference to the role of graphite, Geochim. Cosmochim. Acta 28 (1964) 717–729.
[34] S. Karato, Plasticity-crystal structure systematics in dense oxides and its implications for the creep strength of the Earth's deep interior: a preliminary result, Phys. Earth Planet. Inter. 55 (1989) 234–240.